Chemosphere 224 (2019) 220–227

Contents lists available at ScienceDirect

Chemosphere

journal homepage: www.elsevier.com/locate/chemosphere

Facile modification of activated carbon with highly dispersed nano-sized α-Fe_2O_3 for enhanced removal of hexavalent chromium from aqueous solutions

Bing Li [a], Weizhao Yin [b], Meng Xu [c], Xueyun Tan [a], Ping Li [a], Jingjing Gu [a], Penchi Chiang [a], Jinhua Wu [a, d, e, *]

[a] School of Environment and Energy, South China University of Technology, Guangzhou, 510006, PR China
[b] School of Environment, Jinan University, Guangzhou, 510632, PR China
[c] Poten Environment Group Co., Ltd, Beijing, 100082, PR China
[d] The Key Laboratory of Pollution Control and Ecosystem Restoration in Industry Clusters, Ministry of Education, Guangzhou, 510006, PR China
[e] The Key Laboratory of Environmental Protection and Eco-Remediation of Guangdong Regular Higher Education Institutions, Guangzhou, 510006, PR China

HIGHLIGHTS

- Nano-sized α-Fe_2O_3 was homogeneously distributed on activated carbon.
- Cr(VI) was removed via adsorption, reduction and co-precipitation mechanism.
- The nFe_2O_3@AC composite has good stability and reusability.

GRAPHICAL ABSTRACT

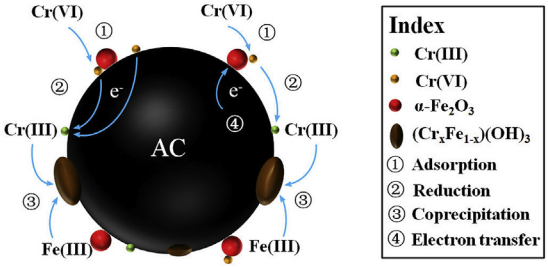

ARTICLE INFO

Article history:
Received 8 January 2019
Received in revised form
15 February 2019
Accepted 18 February 2019
Available online 19 February 2019

Handling Editor: Y Yeomin Yoon

Keywords:
Hematite
Chromium
Activated carbon
Modification

ABSTRACT

Activated carbon-coated α-Fe_2O_3 nanoparticles (nFe_2O_3@AC) were synthesized by a facile impregnation method to enhance hexavalent chromium (Cr(VI)) removal from water. The SEM images confirmed that α-Fe_2O_3 particles ranging from 90 to 500 nm were dispersedly loaded on the AC, which successfully amended Cr(VI) removal. The nFe_2O_3@AC was able to remove Cr(VI) with a 3 times higher efficiency of 94% in comparison with the AC. After adsorption, Cr(VI) reduction coupled with AC oxidation and low soluble $(Cr_xFe_{1-x})(OH)_3$ precipitates were eventually formed. The Cr(VI) removal process was pH-dependent and could be well fitted to pseudo second-order kinetics. The nFe_2O_3@AC could be easily regenerated by 0.1 M HCl and showed a good stability as an 80% Cr(VI) removal efficiency was recorded after 4 desorption-adsorption cycles. In addition, this composite had a promising potential for repeated utilization because the AC of the adsorbed nFe_2O_3@AC could be refreshed and remodified with nFe_2O_3 after stripping all the nFe_2O_3 and $(Cr_xFe_{1-x})(OH)_3$ precipitates from its surface by 1 M HCl and a Cr(VI) removal efficiency of 86% could be achieved. Our results demonstrated that the use of nFe_2O_3 is an efficient and promising method to modify AC and enhance Cr(VI) removal form aqueous solutions.

* Corresponding author. School of Environment and Energy, South China University of Technology, Guangzhou, 510006, PR China.
E-mail address: jinhuawu@scut.edu.cn (J. Wu).

https://doi.org/10.1016/j.chemosphere.2019.02.121
0045-6535/

1. Introduction

Chromium is a toxic metal frequently founded in the environment. It is derived from a variety of industrial processes (e.g., leather tanning, wood processing, metal smelting, textile dyeing and plating) due to the leakage of industrial wastewater and improper practices of industrial sludge disposal (Wang et al., 2010; Wu et al., 2012), causing serious pollution in water environment. In nature environments, trivalent (Cr(III)) and hexavalent (Cr(VI)) are the most common oxidation states of chromium (Lyu et al., 2017). Cr(III) is easily adsorbed by natural clays and precipitates as $Cr(OH)_3$, resulting in significant decrease of its mobility and toxicity (Jiang et al., 2019). While Cr(VI) has a higher solubility and mobility, which can be accumulated in living organisms (Dubey and Gopal, 2009), causing serious threat to human health because of its carcinogenic, mutagenic and teratogenic properties (Vasudevan et al., 2011; Rajput et al., 2016). Therefore, Cr(VI) was identified as a priority pollutant by many countries, and a mandatory discharge limit of 0.05 mg/L in surface water was prescribed by the Ministry of Ecological and Environmental Protection of China (Lyu et al., 2017). It is hence urgent to develop efficient and cost-effective new materials to adsorb Cr(VI) and/or reduce it to Cr(III), thus minimizing its adverse impact on the environment.

During the past decades, various technologies including chemical reduction and precipitation, solvent extraction, ion exchange, membrane filtration, electro deposition and bio-reduction have been applied to treat Cr(VI)-contaminated water (Barrera-Diaz et al., 2012; Dima et al., 2015). However, these methods have various technical or economic defects (e.g., toxic metal sludge generation, incomplete removal and high operational cost). Adsorption has been proved to be a simple, efficient and costless process for the removal of chromium from water (Mohan and Pittman, 2006; Wang et al., 2015b, 2015c; Norouzi et al., 2018). Considering the cost and operation, activated carbon (AC) as an environmentally friendly adsorbent is intensively applied for the removal of organic and inorganic pollutants from aqueous solutions because of its porous structure, high surface area and multiple functional groups (e.g., hydroxyl and carboxyl) (Rivera-Utrilla et al., 2011; Tovar-Gomez et al., 2015). For the adsorption of Cr(VI) onto AC, it is reported that the reduction of Cr(VI) to Cr(III) may happen during the adsorption process since Cr(VI) is a strong oxidant (Espinoza-Quinones et al., 2010; Cruz-Espinoza et al., 2012; Di Natale et al., 2015). The obtained Cr(III) is ready to precipitate due to its low solubility, and therefore enhancing the overall Cr removal from solution (Gheju and Balcu, 2011). However, both the functional groups on AC surface and Cr(VI) ions are negatively charged in aqueous solution, resulting in a poor adsorption capacity of AC for Cr(VI), the value usually blow 10 mg/g due to electrostatic repulsion (Rivera-Utrilla et al., 2011; Bhatnagar et al., 2013; Tounsadi et al., 2016).

Recently, several approaches have been developed to modify AC using acids, oxidants and metal oxides to enhance its oxygen-containing functional groups and decrease electrostatic repulsion for Cr(VI) adsorption (Babel and Kurniawan, 2004; Huang et al., 2009; Yang et al., 2017b). It is reported that magnetite and iron-modified AC has showed significant improvement on Cr(VI) removal due to the introduction of acidic functional groups and iron reduction (Liu et al., 2012; Nethaji et al., 2013). Hematite (α-Fe_2O_3) is another promising iron oxide in the environment and has attracted considerable attention because of several advantages (e.g., low cost, natural abundance and non-toxicity) (Cheng et al., 2015; Wang et al., 2015a; Liu et al., 2017). In comparison with Fe^0 and Fe_3O_4, α-Fe_2O_3 is more stable in the environment and can be easily produced by chemical processes. Since Cr(VI) species are negatively charged, they can be bounded onto α-Fe_2O_3 by electrostatic attraction or complexation due to the ferric oxide groups on the α-Fe_2O_3 surface (Wang et al., 2015a). However, the adsorption efficiency of iron oxides is determined by particle sizes and surface areas (Xiao et al., 2015; Yang et al., 2017a). Exploration of iron oxide nanoparticles (IONPs) as ideal adsorbents is of increasing interest to increase the reactivity of iron oxides. However, high specific surface energy or magnetic force leads to particles aggregation and settlement which significantly diminish their reactivity during application, thus resulting in an inefficient removal performance (Wu et al., 2012). Meanwhile, difficult separation of IONPs from solution leads to the rising of operational cost for post-treatments (e.g, flocculation and sedimentation). To overcome these limitations, loading IONPs onto a carrier such as AC and nanotube potentially provides a promising approach (Nethaji et al., 2013; Wan et al., 2017). Ferric ions can be easily adsorbed onto AC due to their positive charges, therefore loading nano-sized α-Fe_2O_3 onto AC (nFe_2O_3@AC) may enhance its dispersion. This composite is expected to prevent the aggregation of nFe_2O_3 particles, meanwhile change the surface charge of AC by loading the nFe_2O_3 (Jin et al., 2011). Subsequently, the adsorption capacity of AC for Cr(VI) will be improved by this modification. With this respect, the modified AC could be an effective and cost-effective material for Cr(VI) removal from water.

In this study, nFe_2O_3 was employed to modify AC (nFe_2O_3@AC) via a simple and cost-effective impregnation method to form nFe_2O_3@AC composite which would then be used for removing Cr(VI) from aqueous solutions. Surface characterization techniques were employed to analyze the amended Cr(VI) removal mechanism. Cycling tests were also designed to assess the stability and reusability of nFe_2O_3@AC composites.

2. Materials and methods

2.1. Adsorbent preparation

A facile impregnation method was employed to synthesize nano-sized hematite-modified activated carbon (nFe_2O_3@AC) (Wu et al., 2013). In brief, 5 g of AC (0.1 mm, 777 $m^2 \cdot g^{-1}$) was mixed with 27 g of $FeCl_3 \cdot 6H_2O$ in deionized water (200 mL) by a magnetic stirrer for 24 h at 25 °C. The mixture was filtered and rinsed to neutral with deionized water. Subsequently, the residue was dried at 103 °C for 12 h and calcinated at 350 °C for 2 h. The amount of iron oxides loading on the AC was determined to be 2.2% by dissolving the iron oxides into 1 M HCl, and then sent for iron measurement. Unsupported nano-sized hematite (nFe_2O_3) was used as a control and prepared via the method reported by Schwertmann (Schwertmann and Cornell, 2000).

2.2. Adsorption, desorption and reusability experiments

Conical flask reactors (150 mL) were used for batch adsorption experiments, which contained 100 mL Cr(VI) solution at a concentration of 25 $mg \cdot L^{-1}$. The original solution pH value was regulated by 0.1 M H_2SO_4 or NaOH during the pH effect experiment. After adsorbents addition and capping with rubber plugs, the flasks were agitated at 120 rpm, 25 °C in an isothermal shaker for a sufficient time to reach equilibrium. Two milliliter sample was collected at regular intervals by a syringe and measured the Cr(VI) concentration after filtration with a 0.45 μm membrane. The final pH and iron concentrations were detected after reaction.

Hydrochloric acid solution was used as eluents for desorption and reusability test. During the desorption test, the desorbed nFe_2O_3@AC by 0.1 M HCl (120 rpm, 4 h) was filtered and reused at a dosage of 2 $g \cdot L^{-1}$ and a Cr(VI) concentration of 25 $mg \cdot L^{-1}$ for Cr(VI) adsorption. The leaching iron and Cr(VI) concentrations of the

filtrate were measured. After 4 consecutive runs, all the nFe_2O_3 and $(Cr_xFe_{1-x})(OH)_3$ precipitates were stripped using 1 M HCl, and then the nFe_2O_3@AC was regenerated with the above impregnation method for reusability test.

2.3. Analytical methods

An UV–visible spectrophotometer (UV2300, Shanghai, China) was employed to measure the aqueous concentrations of Cr(VI) and ferric iron by following the 1,5-diphenylcarbazide spectrophotometric method (Jia et al., 2018) and the 1,10-phenanthroline colorimetric method (Zhong and Yang, 2012), respectively. A pH meter (PHS-3C, Sanxin, China) was used for pH measurement and the pH_{pzc} of the adsorbents was determined according to the pH drift method (Strelko and Malik, 2002). The mineral composition of the samples was determined on an X-ray diffractometer (D8, Bruker) with X-ray source of Cu-Kα radiation. The scanning electron microscopy (SEM) and energy dispersive X-Ray spectroscopy (EDS) was performed by a Hitachi S-4500 scanning electron microscope. The valent change of Cr(VI) after Cr(VI) adsorption was analyzed by X-ray photoelectron spectroscopy (XPS) (K-Alpha, Thermo Fisher Scientific) with a Kα-Al radiation. Fourier transform infrared spectrum (FTIR) (Nicolet 6700, Thermo Fisher Scientific) was used to identify the change of oxygen-containing functional groups on the AC after Cr(VI) adsorption. For the specific surface areas and pore diameters, they were measured based on adsorption/desorption isotherms at 77 K using a surface area analyzer (ASAP, 2020; Micromeritics).

2.4. Data analysis

Two kinetic models (pseudo-first and pseudo-second order reaction kinetics) were used to fit the adsorption data by Eqs. S1 and S2, respectively. The intraparticle-diffusion model (Weber-Morris model) was employed to analyze the rate limiting step of the Cr(VI) adsorption, as expressed in Eq. S3. And the Langmuir and Freundlich isotherm models were used to describe Cr(VI) adsorption by Eqs. S4 and S5, respectively.

Cr(VI) removal efficiency (R, %) and adsorption capacity (q, $mg \cdot g^{-1}$) were calculated according to Eqs. (1) and (2), respectively.

$$R = (C_0 - C_t) / C_0 \times 100\% \quad (1)$$

$$q = (C_0 - C_t) \times V / m. \quad (2)$$

where C_0 ($mg \cdot L^{-1}$) and C_t ($mg \cdot L^{-1}$) are Cr(VI) concentrations at initial time and reaction time (t), respectively; V (L) and m (g) are the volume of Cr(VI) solution and adsorbent dosage, respectively.

The Cr(VI) desorption efficiency (D, %) and leaching iron rate (L, %) were calculated using Eqs. (3) and (4), respectively.

$$D = (\text{desorbed Cr(VI)}) / (\text{adsorbed Cr(VI)}) \times 100\% \quad (3)$$

$$L = (\text{leached iron}) / (\text{loaded iron}) \times 100\% \quad (4)$$

3. Results and discussion

3.1. Characterization of adsorbents

Fig. 1 shows the XRD patterns of the nFe_2O_3, AC and nFe_2O_3@AC.The nFe_2O_3@AC had a similar XRD pattern to the nFe_2O_3 according to the conspicuous diffraction peaks at 24.3°, 33.5°, 35.8°, 40.9°, 49.7°, 54.3°, 57.7°, 62.6°, and 64.1°, respectively,

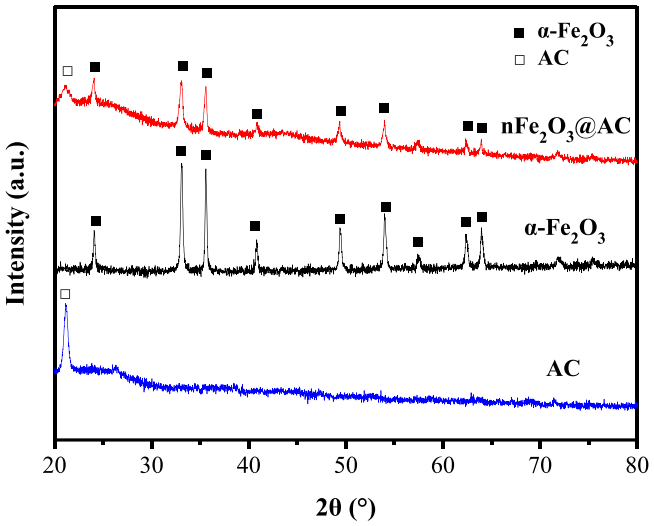

Fig. 1. The X-ray diffraction patterns of absorbents.

indicating the structure of hematite on the nFe_2O_3@AC (α-Fe_2O_3, JCPDS 33-0664) (Liu et al., 2017). This pattern further demonstrated good crystallinity of the samples and successful synthesis of the Fe_2O_3@AC composite. An additional peak is observed in the nFe_2O_3@AC sample at 22° because of the AC (Shinde et al., 2017). The peak was broader than that of the AC alone, indicating the presence of smaller particles (Venkateswarlu et al., 2016), such as nFe_2O_3 particles in this study.

As shown in the SEM images (Fig. 2), unsupported α-Fe_2O_3 particles with a size of 50–100 nm were obtained. Nano-sized α-Fe_2O_3 (nFe_2O_3) ranging from 90 to 500 nm was dispersedly loaded on the modified AC. After Cr(VI) adsorption, irregular nFe_2O_3 particles became spherical, with a diameter of 100–500 nm. According to the morphology features, these particles were primarily identified to be $(Cr_xFe_{1-x})(OH)_3$ precipitates (Lo et al., 2006), since the surface-bounded Cr(VI) is likely to be reduced to Cr(III) by the functional groups such as ≡C-OH on the AC (Di Natale et al., 2015; Norouzi et al., 2018).

Table 1 summarized element composition (revealed by EDS), surface area, and pore diameter of the adsorbents. The element composition of the AC and the nFe_2O_3 was determined to be 72.9% C, 27.1% Oxygen and 70% Fe, 30% O, respectively. After the loading of nFe_2O_3, the C on the AC surface was decreased to 62.5% and the O, Fe percentage were correspondingly increased to 34.3% and 3.2%, respectively. It was consistent with the XRD results which showed the conspicuous diffraction peaks of the α-Fe_2O_3 in the modified AC. In addition, 2.8% Cr was founded in the elemental composition of the precipitates on the nFe_2O_3@AC, further demonstrated successful adsorption of Cr(VI) by the nFe_2O_3@AC. Due to the adsorbed Cr(VI) and its conversion to $(Cr_xFe_{1-x})(OH)_3$ precipitates, the O percentage of the nFe_2O_3@AC was further increased to 40.9%. After adsorption, the C and Fe of the nFe_2O_3@AC were decreased from 62.5% to 53.4% and from 3.2% to 2.9%, respectively. It was attributed to the dilution effect of Cr(VI) and $(Cr_xFe_{1-x})(OH)_3$ precipitates on the surfaces of the nFe_2O_3@AC (Wang et al., 2015a).

Although the pore diameter of the AC was decreased from 5.0 nm to 4.9 nm due to the blocking effect after loading nFe_2O_3 (Table 1), the surface area of the nFe_2O_3@AC ($811\ m^2 \cdot g^{-1}$) was higher than the sum of the AC ($777\ m^2 \cdot g^{-1}$) and the unsupported nFe_2O_3 ($22.6\ m^2 \cdot g^{-1}$), probably due to the presence of supported nFe_2O_3 that provided extra specific surface area and compensated the occupied surface area by themselves. Due to the formation of Cr

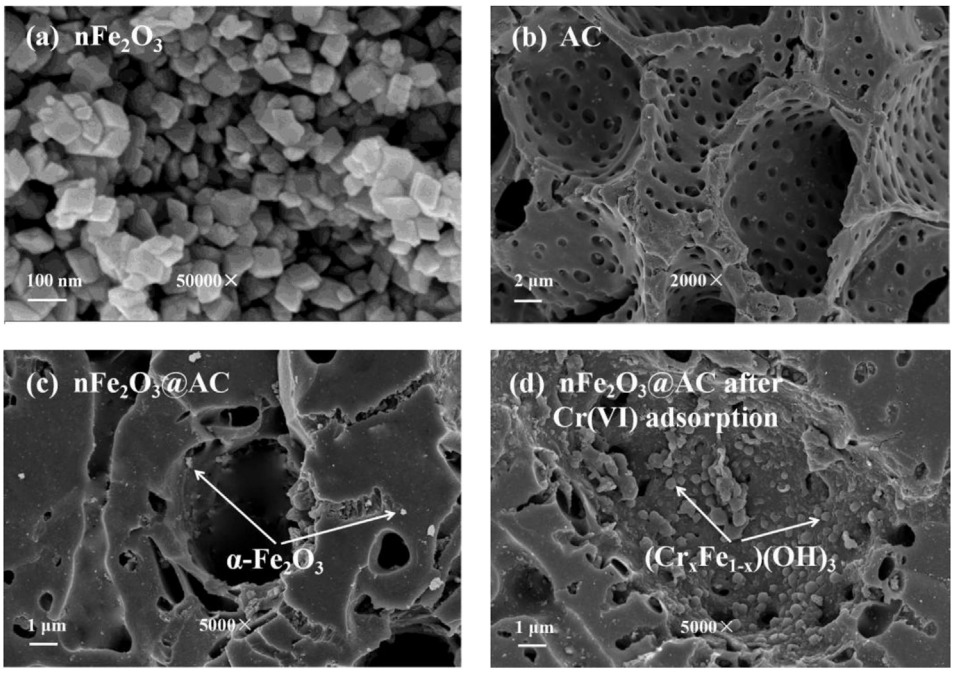

Fig. 2. The SEM images of (a) nFe_2O_3, (b) AC, (c) nFe_2O_3@AC and (d) nFe_2O_3@AC after Cr(VI) adsorption.

Table 1
The BET surface area, pore diameter and elemental composition of adsorbents before and after Cr(VI) adsorption. nFe_2O_3@AC*: nFe_2O_3@AC after Cr(VI) adsorption; NA: not detected.

Sample	Element (wt%)				BET surface area ($m^2 \cdot g^{-1}$)	Pore diameter (nm)
	C	O	Fe	Cr		
AC	72.9	27.1	NA	NA	777	5.0
nFe_2O_3	NA	70	30	NA	26.2	0.7
nFe_2O_3@AC	62.5	34.3	3.2	NA	811	4.9
nFe_2O_3@AC*	53.4	40.9	2.9	2.8	724	4.6

precipitates, a slight decrease of surface area and pore diameter was observed in the nFe_2O_3@AC after adsorption.

The results indicated that nFe_2O_3 was successfully loaded onto AC, which formed the nFe_2O_3@AC.

3.2. Cr(VI) removal test

The nFe_2O_3@AC composite was tested for Cr(VI) removal with AC and nFe_2O_3 as controls. Fig. 3 shows that the nFe_2O_3 just removed 15% of Cr(VI) in 600 min. Since easy aggregation of nFe_2O_3 would occur in solution due to high specific surface energy, Cr(VI) adsorption was limited. Similar to the nFe_2O_3 system, the pristine AC only provided a 23% Cr(VI) removal in 600 min, demonstrating that AC has weak affinity to Cr(VI), which might be due to electrostatic repulsion. In the nFe_2O_3@AC system, a much higher Cr(VI) removal efficiency of 94% was recorded in 600 min, which is 3 times higher than that of the AC alone. The nFe_2O_3@AC showed stronger affinity to Cr(VI) due to its positively charged surface from the nFe_2O_3. Such surface could afford strong adsorption ability for heavy metal via electrostatic attraction, complexation and co-precipitation (Liu et al., 2012; Shinde et al., 2017). Meanwhile, as shown in the SEM and BET results (Fig. 2 and Table 1), since the nFe_2O_3 was dispersedly loaded on the AC, higher surface areas were thereafter obtained in the nFe_2O_3@AC system than those of the nFe_2O_3 system, amending the Cr(VI) adsorption by providing larger amount of reactive sites.

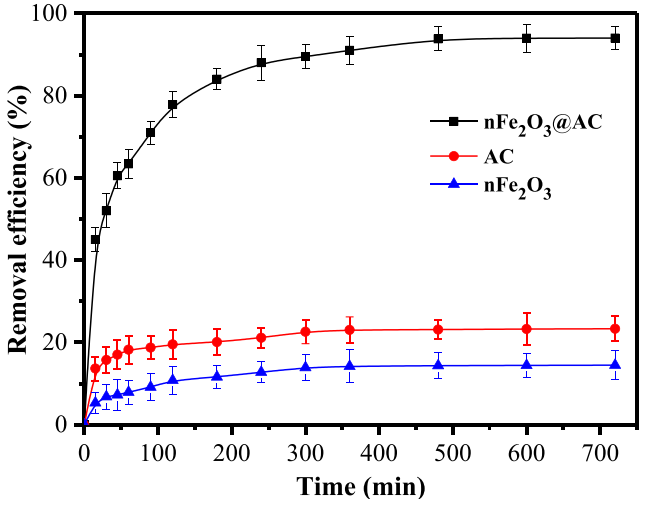

Fig. 3. Cr(VI) removal by different adsorbents (0.04 $g \cdot L^{-1}$ of nFe_2O_3, 2 $g \cdot L^{-1}$ of AC and nFe_2O_3@AC, 25 $mg \cdot L^{-1}$ of Cr(VI) at initial pH 5.6 and 25 °C).

The Cr(VI) removal data was fitted to two kinetic models (pseudo first-order and pseudo second-order kinetic models), respectively (Table S1). It can be seen that the experimental values ($q_{e,\ exp}$) were similar to the calculated values ($q_{e,c}$) of the pseudo

second-order kinetic model, and the R^2 values (0.99) were higher than those of the pseudo first-order kinetic one (0.79 and 0.92), indicating that the Cr(VI) removal fitted well with the pseudo second-order model in this study. This result is consistent with other research using chestnut shell AC (Niazi et al., 2018), $FeCl_3$-modified (Sun et al., 2014) AC and Fe_3O_4-modified AC (Nethaji et al., 2013) as adsorbents. It indicated that the Cr(VI) adsorption rate was controlled by chemisorptions. It also suggested that the sharing or exchanging electrons in the interfaces might exist during Cr(VI) adsorption onto the nFe_2O_3@AC (Wu et al., 2012). In addition, the limiting step of the Cr(VI) adsorption was analyzed by using the Weber and Morris model. As seen in Fig. S1 and Table S2, the adsorption data of the Cr(VI) could be fitted to two stages, where the first stage was the surface/instantaneous adsorption process, subsequently the gradual adsorption stage was provided in the second stage (Aigbe et al., 2018). And the C values of each stage were not zero, indicating that the rate limiting step of Cr(VI) adsorption by the AC and the nF_2O_3@AC was not just intraparticle diffusion, other step could be existed (Kong et al., 2019).

It should be noted that Cr(VI) has a higher standard reduction potential of 1.33 V (acidic condition) than that of HNO_3 (0.96 V) (Mishra et al., 2015; Wang et al., 2017) and HNO_3 is widely used to modify AC to increase the number of acidic function groups on its surface for enhanced Cr(VI) adsorption (Huang et al., 2009). It can be expected that Cr(VI) reduction could be coupled with AC oxidation, where oxygen-containing groups and Cr(III) species were formed (Liu et al., 2012). The resultant Cr(III) is prone to precipitate for its low solubility (Gheju and Balcu, 2011; Shen et al., 2016) and the reduction of Cr(VI) to Cr(III) by AC is considered to be a main reason for outstanding Cr(VI) removal since the nFe_2O_3@AC was successfully synthesized according to XRD and SEM analysis. XPS and FTIR spectra was thereafter collected to further confirm the coupled AC oxidation and Cr(VI) reduction. According to Fig. 4, the C-OH vibration (3420 cm^{-1}) of the AC significantly decreased while the C-O vibration (1610 cm^{-1}) strengthened after Cr(VI) adsorption, indicating the oxidation of AC by Cr(VI) and the functional groups (≡C-OH) of the AC could function as reductant to reduce the surface-bounded Cr(VI) (Rangabhashiyam and Selvaraju, 2015). The XPS spectra (Fig. 5) showed that Cr(III) species distributed on the nFe_2O_3@AC after adsorption were confirmed by measuring the binding energy at 586.5 and 577.2 eV (Mu et al., 2015; Mortazavian et al., 2019), while only Cr(VI) species were observed on the sample

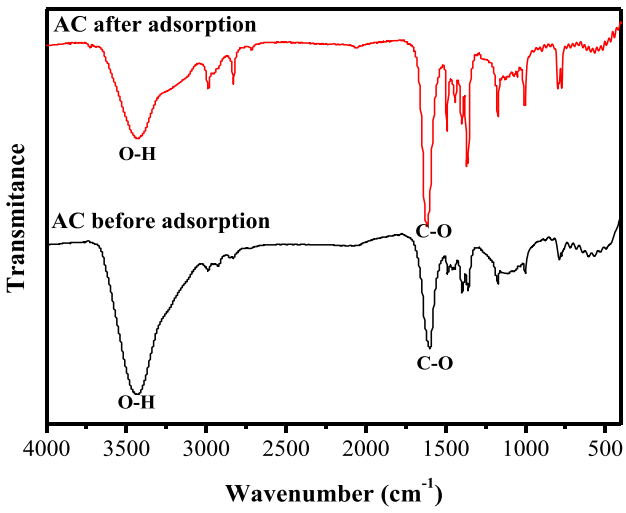

Fig. 4. The FTIR spectra of AC before and after Cr(VI) adsorption (2 g·L^{-1} of AC, 25 mg·L^{-1} of Cr(VI) at initial pH 5.6 and 25 °C).

without AC. According to the above results, a possible Cr(VI) removal mechanism using nFe_2O_3@AC could be deduced. In the solution, Cr(VI) was initially adsorbed onto nFe_2O_3@AC via complexation and electrostatic attraction. Then the Cr(VI) was directly reduced by AC (Espinoza-Quinones et al., 2010) or through the nFe_2O_3 as electron shuttles (Williams and Scherer, 2004; Katz et al., 2012; Mu et al., 2015) because iron oxides (0.77 V) (Chakraborty et al., 2010) have a much lower reduction potential than that of $Cr_2O_7^{2-}/Cr^{3+}$ (1.33 V) (Mishra et al., 2015) and the electrons on the nFe_2O_3 surfaces transferred from the AC could reduce Cr(VI) to Cr(III). Subsequently, according to SEM and BET results, partial Cr(III) species precipitated to form chromium hydroxides (Shen et al., 2016) or Cr(III)-Fe(III) precipitates since Cr(III) and Fe(III) ions have similar ionic radius of 0.064 nm and same charge (Zhong et al., 2017). Finally, Cr(VI) could be trapped at the surfaces of the nFe_2O_3@AC and further encapsulated into the crystalline structure of the iron oxides which eventually converted to spherical phase particles as shown in Fig. 2.

Furthermore, Fig. 3 shows that a rapid adsorption occurred during the first 120 min, followed by a much slower phase until the system reached the adsorption equilibrium after roughly 600 min due to the outer diffusion and the interior complexation (Dai et al., 2016). Thus, 600 min was selected as the reaction time for further experiments.

3.3. Effect of pH

The pH values from 3.0 to 11.0 were applied to the pH test and the result is present in Fig. 6. It can be seen that Cr(VI) removal increased from 10% to 40%, and from 17% to 99% using AC and nFe_2O_3@AC, respectively when the pH values were decreased from 11 to 3. Obviously, the adsorption process was highly pH-dependent and higher removal efficiencies could be achieved under acidic conditions, particularly in the nFe_2O_3@AC system. This phenomenon is related to various forms of Cr(VI) and surface properties of absorbents at different pH values (Rajput et al., 2016). Generally, Cr(VI) exists as $Cr_2O_7^{2-}$, CrO_4^{2-} and $HCrO_4^-$ in aqueous solutions depending on pH values (Wu et al., 2012). $HCrO_4^-$ is the common form at pH 1–6.5, while $Cr_2O_7^{2-}$ and CrO_4^{2-} are the primary forms under neutral and alkaline conditions. Besides, the surface charge of the nFe_2O_3@AC is positive or negative depending on pH values since the pH_{pzc} of the AC and the nFe_2O_3@AC was calculated to be 8.0 and 6.9, respectively (Figs. S2 and S3). Surface protonation of AC and nFe_2O_3@AC would occur under acidic conditions (Lazaridis and Charalambous, 2005; Huang et al., 2009). Subsequently, enhanced Cr(VI) adsorption was achieved because of strong electrostatic attraction between the negatively charged Cr(VI) species and the positively charged surfaces of the adsorbents (Prabhakaran et al., 2009). As pH values increased, the functional groups of the nFe_2O_3@AC were deprotonated gradually and the surface of nFe_2O_3@AC was even negatively charged when pH exceeded pH_{pzc} (6.9). This led to strong exclusion between Cr(VI) and nFe_2O_3@AC. Thereafter, Cr(VI) removal was inhibited. Under alkaline conditions, excess OH^- also competed with CrO_4^{2-} and $Cr_2O_7^{2-}$ for adsorption sites and therefore suppressed Cr(VI) adsorption (Zhuang et al., 2014). Hence, the adsorption of Cr(VI) by the nFe_2O_3@AC was favorable under acidic conditions.

Since iron ion would be leached in weak acid environment, the leaching iron rate after the reactions was evaluated. As shown in Fig. 6, when the pH was decreased from 11 to 3, aqueous iron concentrations increased from 1.7% to 10.5%. This relatively low leaching iron rate indicated that the nFe_2O_3@AC can be a long lasting adsorbent applied for Cr(VI) removal from waters. The initial pH 5.6 could function as an optimum pH since a relative low leaching iron rate and a high Cr(VI) removal was recorded under

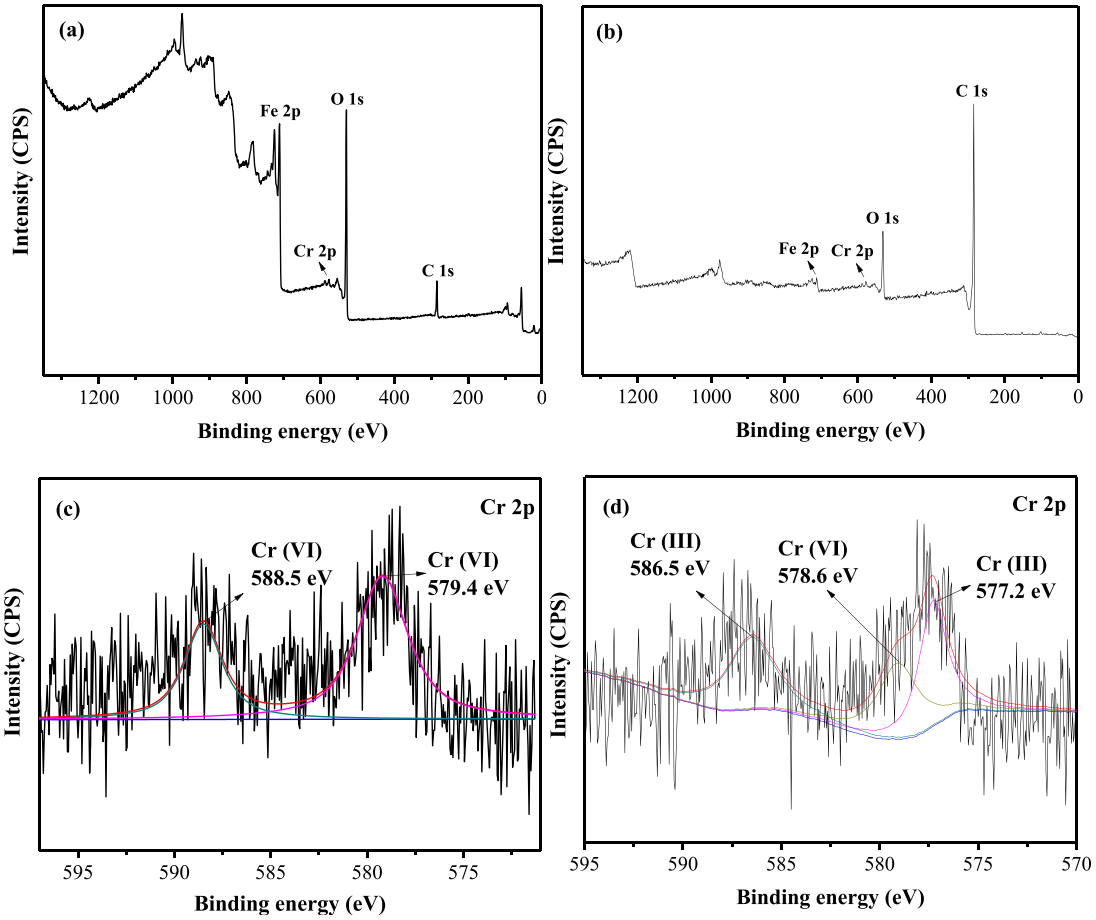

Fig. 5. The XPS spectra of (a) nFe_2O_3, (b) nFe_2O_3@AC, the Cr 2p of (c) nFe_2O_3 and (d) nFe_2O_3@AC after Cr(VI) adsorption (0.04 g·L^{-1} of nFe_2O_3, 2 g·L^{-1} of AC and nFe_2O_3@AC, 25 mg·L^{-1} of Cr(VI) at initial pH 5.6 and 25 °C).

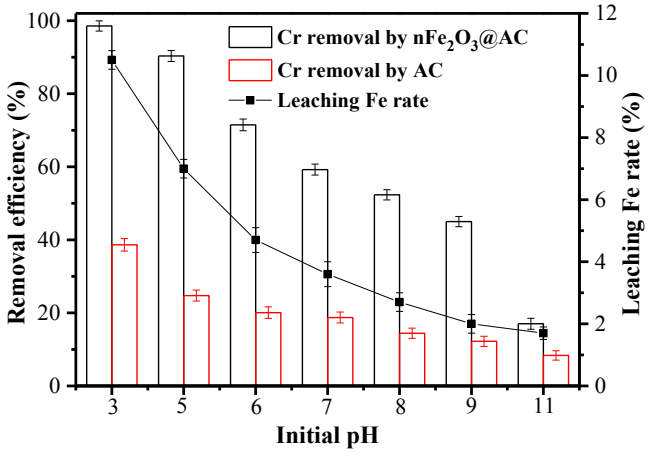

Fig. 6. The effect of initial pH on Cr(VI) adsorption (2 g·L^{-1} of AC and nFe_2O_3@AC, 25 mg·L^{-1} of Cr(VI) at 25 °C).

this condition.

3.4. Adsorption isotherms

The adsorption isotherms were established by setting the initial Cr(VI) concentrations from 5 to 500 mg·L^{-1} and the results are presented in Fig. S4. The equilibrium adsorption capacity (q_e) of the adsorbents increased with equilibrium Cr(VI) concentration (C_e) and reached a stable state when C_e above 300 mg·L^{-1} due to the saturation of adsorption sites at high Cr(VI) concentrations (Su et al., 2019).

Two isotherm models (the Langmuir and the Freundlich) were used to describe Cr(VI) adsorption by the nFe_2O_3@AC and the AC. The fitting parameters are presented in Table 2. The results showed a better fitting to the Langmuir model than the Freundlich model with a correlation coefficient (R^2) >0.99 (Table 2), indicating that Cr(VI) removal by the nFe_2O_3@AC was a monolayer adsorption (Yilmaz et al., 2005). This was attributed to the high dispersion of oxygen-containing functional groups and nFe_2O_3 particles on the surfaces of AC. In addition, according to the Langmuir model, the nFe_2O_3@AC had a much higher Langmuir maximum adsorption capacity of 32.1 mg·g^{-1} than that of the AC (5.2 mg·g^{-1}), demonstrating that the ability of the AC for Cr(VI) adsorption was remarkably improved after nFe_2O_3 modification. This Cr(VI) adsorption capacity is competitive among the previously reported absorbents (Table S3), such as hematite (2.3 mg·g^{-1}) (Ajouyed et al.,

Table 2
The Langmuir and Freundlich model parameters for the adsorption of Cr(VI).

Adsorbent	Langmuir			Freundlich		
	K_L (L·mg^{-1})	q_m (mg·g^{-1})	R^2	K_F (L·g^{-1})	n	R^2
AC	0.02	5.2	0.995	0.45	2.5	0.972
nFe_2O_3@AC	0.05	32.1	0.997	2.59	2.4	0.931

2010), AC (6.4 mg·g^{-1}) (Huang et al., 2009), HNO_3-modified AC (16.1 mg·g^{-1}) (Huang et al., 2009), Fe-modified AC (11.8 mg·g^{-1}) (Liu et al., 2010) α-Fe_2O_3-modifiyed nanofiber (16.2 mg·g^{-1}) (Ren et al., 2013) and Fe_3O_4-modified AC (57.4 mg·g^{-1}) (Nethaji et al., 2013). This comparison indicates that the nFe_2O_3@AC is of great potential in the Cr(VI) removal from aqueous solution.

3.5. Desorption and regeneration studies

Desorption (leaching) and regeneration tests were performed to assess the stability and reusability of the nFe_2O_3@AC. The results of the desorption study (Fig. 7) showed that the nFe_2O_3@AC was stable in acidic solutions as only 23.8% Fe was released into solution after 4 runs of desorption process. While, after 4 cycles operation, the desorbed nFe_2O_3@AC maintained a high Cr(VI) removal efficiency of 80%, which was slightly decreased (14%) from the first removal efficiency of 94%, possibly due to the increased numbers of acidic function groups such as carboxyl groups that could interact with Cr(VI) via complexation after acid treatment and this was supported by its decrease of pH_{pzc} from 6.9 to 5.0 after acid activation (Figs. S3 and S5). Similar activated effect was obtained by Huang et al. (2009) when using HNO_3 to modify AC for enhanced Cr(VI) adsorption. In addition, pore dredging and surface cleaning effect of HCl was also favorable for enhanced Cr(VI) adsorption of the nFe_2O_3@AC after acid activation.

After 4 cycles of operation, the deactivated nFe_2O_3@AC was regenerated by adding 1 M HCl which striped all the nFe_2O_3 and $(Cr_xFe_{1-x})(OH)_3$ precipitates on its surfaces and pores, subsequently reloaded with nFe_2O_3. A removal efficiency of 86% was obtained by the regenerated nFe_2O_3@AC. It indicated that the nFe_2O_3@AC had an excellent stability and showed a great potential for repeated utilization in Cr(VI) removal with a simple and convenient regeneration method.

4. Conclusions

A nFe_2O_3@AC adsorbent was synthesized with a simple impregnation method by loading highly dispersed nano-sized α-Fe_2O_3 particles onto AC. Surface characterization revealed that nano-sized α-Fe_2O_3 particles were dispersedly loaded on the AC, which decreased the pH_{pzc} of the AC and significantly enhanced its Cr(VI) adsorption capacity since nFe_2O_3 has a strong affinity to Cr(VI) due to electrostatic attraction. The adsorbed Cr(VI) was reduced to Cr(III) by the AC and the resultant Cr(III) subsequently precipitated as low soluble Cr(III) or Cr(III)-Fe(III) hydroxides, which facilitated overall Cr(VI) removal from solution. Cr(VI) adsorption and sequestration on the nFe_2O_3@AC was an adsorption-reduction mechanism and the synergetic effect between the AC and the nFe_2O_3 enable the nFe_2O_3@AC a 5.2 times higher Cr(VI) removal capacity than that of the AC. The Cr(VI) removal data could be well fitted to the pseudo second-order kinetics and the Langmuir adsorption model, indicating that the adsorption of Cr(VI) onto the nFe_2O_3@AC was a monolayer adsorption. The nFe_2O_3@AC also showed an excellent stability during acid desorption and its regeneration could be achieved after cleaning up all the metal oxides on the AC and reloading nFe_2O_3 particles, making this technique simple and cost-effective during application. In addition, the adsorption of Cr(VI) onto the nFe_2O_3@AC was pH-dependent and high pH inhibited the overall Cr(VI) removal. Our results demonstrated that good stability and reusability will enable the nFe_2O_3@AC to be a promising adsorbent for Cr(VI) removal.

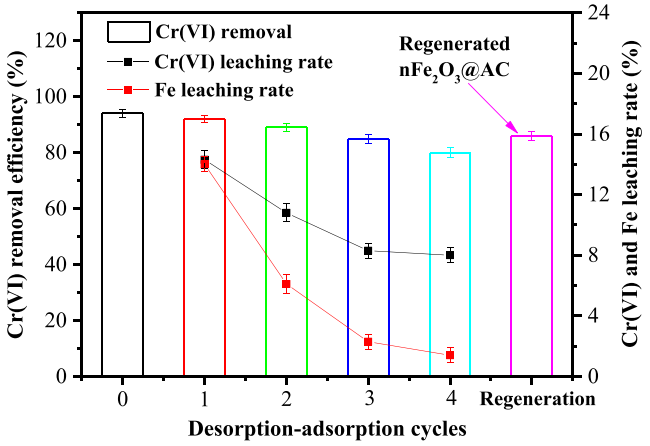

Fig. 7. The Cr(VI) removal efficiencies of recycled and regenerated nFe_2O_3@AC (2 g·L^{-1} of nFe_2O_3@AC, 25 mg·L^{-1} of Cr(VI) at initial pH 5.6 and 25 °C).

Acknowledgments

The authors thank the support from the National Natural Science Foundation of China (41571302, 41807338), the Science and Technology Project of Guangzhou (201803030036), the Water Resource Science and Technology Innovation Program of Guangdong Province (2016-26) and the Fundamental Research Funds for the Central Universities (21618343).

Appendix A. Supplementary data

Supplementary data to this article can be found online at https://doi.org/10.1016/j.chemosphere.2019.02.121.

References

Aigbe, U.O., Das, R., Ho, W.H., Srinivasu, V., Maity, A., 2018. A novel method for removal of Cr(VI) using polypyrrole magnetic nanocomposite in the presence of unsteady magnetic fields. Separ. Purif. Technol. 194, 377–387.
Ajouyed, O., Hurel, C., Ammari, M., Ben Allal, L., Marmier, N., 2010. Sorption of Cr(VI) onto natural iron and aluminum (oxy)hydroxides: effects of pH, ionic strength and initial concentration. J. Hazard Mater. 174, 616–622.
Babel, S., Kurniawan, T.A., 2004. Cr(VI) removal from synthetic wastewater using coconut shell charcoal and commercial activated carbon modified with oxidizing agents and/or chitosan. Chemosphere 54, 951–967.
Barrera-Diaz, C.E., Lugo-Lugo, V., Bilyeu, B., 2012. A review of chemical, electrochemical and biological methods for aqueous Cr(VI) reduction. J. Hazard Mater. 223, 1–12.
Bhatnagar, A., Hogland, W., Marques, M., Sillanpaa, M., 2013. An overview of the modification methods of activated carbon for its water treatment applications. Chem. Eng. J. 219, 499–511.
Chakraborty, S., Bardelli, F., Charlet, L., 2010. Reactivities of Fe(II) on calcite: selenium reduction. Environ. Sci. Technol. 44, 1288–1294.
Cheng, Q., Wang, C.W., Doudrick, K., Chan, C.K., 2015. Hexavalent chromium removal using metal oxide photocatalysts. Appl. Catal. B Environ. 176, 740–748.
Cruz-Espinoza, A., Ibarra-Galvan, V., Lopez-Valdivieso, A., Gonzalez-Gonzalez, J., 2012. Synthesis of microporous eskolaite from Cr(VI) using activated carbon as a reductant and template. J. Colloid Interface Sci. 374, 321–324.
Dai, Y., Hu, Y.C., Jiang, B.J., Zou, J.L., Tian, G.H., Fu, H.G., 2016. Carbothermal synthesis of ordered mesoporous carbon-supported nano zero-valent iron with enhanced stability and activity for hexavalent chromium reduction. J. Hazard Mater. 309, 249–258.
Di Natale, F., Erto, A., Lancia, A., Musrnarra, D., 2015. Equilibrium and dynamic study on hexavalent chromium adsorption onto activated carbon. J. Hazard Mater. 281, 47–55.
Dima, J.B., Sequeiros, C., Zaritzky, N.E., 2015. Hexavalent chromium removal in contaminated water using reticulated chitosan micro/nanoparticles from seafood processing wastes. Chemosphere 141, 100–111.
Dubey, S.P., Gopal, K., 2009. Adsorption of chromium(VI) on low cost adsorbents derived from agricultural waste material: a comparative study (vol 145, pg 465, 2007). J. Hazard Mater. 170, 506-506.
Espinoza-Quinones, F.R., Modenes, A.N., Camera, A.S., Stutz, G., Tirao, G., Palacio, S.M., Kroumov, A.D., Oliveira, A.P., Alflen, V.L., 2010. Application of high resolution X-ray emission spectroscopy on the study of Cr ion adsorption by activated carbon. Appl. Radiat. Isot. 68, 2208–2213.

Gheju, M., Balcu, I., 2011. Removal of chromium from Cr(VI) polluted wastewaters by reduction with scrap iron and subsequent precipitation of resulted cations. J. Hazard Mater. 196, 131–138.
Huang, G.L., Shi, J.X., Langrish, T.A.G., 2009. Removal of Cr(VI) from aqueous solution using activated carbon modified with nitric acid. Chem. Eng. J. 152, 434–439.
Jia, Z.Z., Shu, Y.H., Huang, R.L., Liu, J.G., Liu, L.L., 2018. Enhanced reactivity of nZVI embedded into supermacroporous cryogels for highly efficient Cr(VI) and total Cr removal from aqueous solution. Chemosphere 199, 232–242.
Jiang, B., Gong, Y., Gao, J., Sun, T., Liu, Y., Oturan, N., Oturan, M.A., 2019. The reduction of Cr(VI) to Cr(III) mediated by environmentally relevant carboxylic acids: state-of-the-art and perspectives. J. Hazard Mater. 365, 205–226.
Jin, X., Yu, C., Li, Y., Qi, Y., Yang, L., Zhao, G., Hu, H., 2011. Preparation of novel nano-adsorbent based on organic-inorganic hybrid and their adsorption for heavy metals and organic pollutants presented in water environment. J. Hazard Mater. 186, 1672–1680.
Katz, J.E., Zhang, X., Attenkofer, K., Chapman, K.W., Frandsen, C., Zarzycki, P., Rosso, K.M., Falcone, R.W., Waychunas, G.A., Gilbert, B., 2012. Electron small polarons and their mobility in iron (Oxyhydr)oxide nanoparticles. Science 337, 1200–1203.
Kong, Q.P., Wei, J.Y., Hu, Y., Wei, C.H., 2019. Fabrication of terminal amino hyper-branched polymer modified graphene oxide and its prominent adsorption performance towards Cr(VI). J. Hazard Mater. 363, 161–169.
Lazaridis, N.K., Charalambous, C., 2005. Sorptive removal of trivalent and hex-avalent chromium from binary aqueous solutions by composite alginate-goethite beads. Water Res. 39, 4385–4396.
Liu, W.F., Zhang, J., Zhang, C.L., Ren, L., 2012. Preparation and evaluation of activated carbon-based iron-containing adsorbents for enhanced Cr(VI) removal: mech-anism study. Chem. Eng. J. 189, 295–302.
Liu, W.F., Zhang, J.A., Zhang, C.L., Wang, Y.F., Li, Y., 2010. Adsorptive removal of Cr (VI) by Fe-modified activated carbon prepared from Trapa natans husk. Chem. Eng. J. 162, 677–684.
Liu, Z., Yu, R.T., Dong, Y.P., Li, W., Lv, B.L., 2017. The adsorption behavior and mechanism of Cr(VI) on 3D hierarchical alpha-Fe_2O_3 structures exposed by (001) and non-(001) planes. Chem. Eng. J. 309, 815–823.
Lo, I.M.C., Lam, C.S.C., Lai, K.C.K., 2006. Hardness and carbonate effects on the reactivity of zero-valent iron for Cr(VI) removal. Water Res. 40, 595–605.
Lyu, H.H., Tang, J.C., Huang, Y., Gai, L.S., Zeng, E.Y., Liber, K., Gong, Y.Y., 2017. Removal of hexavalent chromium from aqueous solutions by a novel biochar supported nanoscale iron sulfide composite. Chem. Eng. J. 322, 516–524.
Mishra, S., Lawrence, F., Mallika, C., Pandey, N.K., Srinivasan, R., Mudali, U.K., Natarajan, R., 2015. Kinetics of reduction of nitric acid by electrochemical method and validation of cell design for plant application. Electrochim. Acta 160, 219–226.
Mohan, D., Pittman, C.U., 2006. Activated carbons and low cost adsorbents for remediation of tri- and hexavalent chromium from water. J. Hazard Mater. 137, 762–811.
Mortazavian, S., Saber, A., Hong, J., Bae, J.-H., Chun, D., Wong, N., Gerrity, D., Batista, J., Kim, K.J., Moon, J., 2019. Synthesis, characterization, and kinetic study of activated carbon modified by polysulfide rubber coating for aqueous hex-avalent chromium removal. J. Ind. Eng. Chem. 69, 196–210.
Mu, Y., Wu, H., Ai, Z.H., 2015. Negative impact of oxygen molecular activation on Cr(VI) removal with core-shell Fe@Fe_2O_3 nanowires. J. Hazard Mater. 298, 1–10.
Nethaji, S., Sivasamy, A., Mandal, A.B., 2013. Preparation and characterization of corn cob activated carbon coated with nano-sized magnetite particles for the removal of Cr(VI). Bioresour. Technol. 134, 94–100.
Niazi, L., Lashanizadegan, A., Sharififard, H., 2018. Chestnut oak shells activated carbon: preparation, characterization and application for Cr (VI) removal from dilute aqueous solutions. J. Clean. Prod. 185, 554–561.
Norouzi, S., Heidari, M., Alipour, V., Rahmanian, O., Fazlzadeh, M., Mohammadi-Moghadam, F., Nourmoradi, H., Goudarzi, B., Dindarloo, K., 2018. Preparation, characterization and Cr(VI) adsorption evaluation of NaOH-activated carbon produced from Date Press Cake; an agro-industrial waste. Bioresour. Technol. 258, 48–56.
Prabhakaran, S.K., Vijayaraghavan, K., Balasubramanian, R., 2009. Removal of Cr(VI) ions by spent tea and coffee dusts: reduction to Cr(III) and biosorption. Ind. Eng. Chem. Res. 48, 2113–2117.
Rajput, S., Pittman, C.U., Mohan, D., 2016. Magnetic magnetite (Fe_3O_4) nanoparticle synthesis and applications for lead (Pb^{2+}) and chromium (Cr^{6+}) removal from water. J. Colloid Interface Sci. 468, 334–346.
Rangabhashiyam, S., Selvaraju, N., 2015. Efficacy of unmodified and chemically modified Swietenia mahagoni shells for the removal of hexavalent chromium from simulated wastewater. J. Mol. Liq. 209, 487–497.
Ren, T.Y., He, P., Niu, W.L., Wu, Y.J., Ai, L.H., Gou, X.L., 2013. Synthesis of alpha-Fe_2O_3 nanofibers for applications in removal and recovery of Cr(VI) from wastewater. Environ. Sci. Pollut. Res. 20, 155–162.
Rivera-Utrilla, J., Sanchez-Polo, M., Gomez-Serrano, V., Alvarez, P.M., Alvim-Ferraz, M.C.M., Dias, J.M., 2011. Activated carbon modifications to enhance its water treatment applications. An overview. J. Hazard Mater. 187, 1–23.
Schwertmann, H.C.U., Cornell, R.M., 2000. Iron oxides in the laboratory: preparation and characterization. Clay Miner. 27, 393-393.
Shen, W., Mu, Y., Xiao, T., Ai, Z., 2016. Magnetic Fe_3O_4–FeB nanocomposites with promoted Cr(VI) removal performance. Chem. Eng. J. 285, 57–68.
Shinde, P.S., Mahadik, M.A., Lee, S.Y., Ryu, J., Choi, S.H., Jang, J.S., 2017. Surfactant and TiO2 underlayer derived porous hematite nanoball array photoanode for enhanced photoelectrochemical water oxidation. Chem. Eng. J. 320, 81–92.
Strelko, V., Malik, D.J., 2002. Characterization and metal sorptive properties of oxidized active carbon. J. Colloid Interface Sci. 250, 213–220.
Su, M., Fang, Y., Li, B., Yin, W., Gu, J., Liang, H., Li, P., Wu, J., 2019. Enhanced hex-avalent chromium removal by activated carbon modified with micro-sized goethite using a facile impregnation method. Sci. Total Environ. 647, 47–56.
Sun, Y.Y., Yue, Q.Y., Mao, Y.P., Gao, B.Y., Gao, Y., Huang, L.H., 2014. Enhanced adsorption of chromium onto activated carbon by microwave-assisted H_3PO_4 mixed with Fe/Al/Mn activation. J. Hazard Mater. 265, 191–200.
Tounsadi, H., Khalidi, A., Machrouhi, A., Farnane, M., Elmoubarki, R., Elhalil, A., Sadiq, M., Barka, N., 2016. Highly efficient activated carbon from Glebionis coronaria L. biomass: optimization of preparation conditions and heavy metals removal using experimental design approach. J. Environ. Chem. Eng. 4, 4549–4564.
Tovar-Gomez, R., Moreno-Virgen, M.D., Moreno-Perez, J., Bonilla-Petriciolet, A., Hernandez-Montoya, V., Duran-Valle, C.J., 2015. Analysis of synergistic and antagonistic adsorption of heavy metals and acid blue 25 on activated carbon from ternary systems. Chem. Eng. Res. Des. 93, 755–772.
Vasudevan, S., Lakshmi, J., Sozhan, G., 2011. Studies on the Al-Zn-In-alloy as anode material for the removal of chromium from drinking water in electro-coagulation process. Desalination 275, 260–268.
Venkateswarlu, S., Lee, D., Yoon, M., 2016. Bioinspired 2d-carbon flakes and Fe_3O_4 nanoparticles composite for arsenite removal. ACS Appl. Mater. Interfaces 8, 23876–23885.
Wan, X.Y., Zhan, Y.Q., Long, Z.H., Zeng, G.Y., He, Y., 2017. Core@double-shell struc-tured magnetic halloysite nanotube nano-hybrid as efficient recyclable adsor-bent for methylene blue removal. Chem. Eng. J. 330, 491–504.
Wang, Q., Huang, L.P., Pan, Y.Z., Quan, X., Puma, G.L., 2017. Impact of Fe(III) as an effective electron-shuttle mediator for enhanced Cr(VI) reduction in microbial fuel cells: reduction of diffusional resistances and cathode overpotentials. J. Hazard Mater. 321, 896–906.
Wang, S.S., Gao, B., Zimmerman, A.R., Li, Y.C., Ma, L., Harris, W.G., Migliaccio, K.W., 2015a. Removal of arsenic by magnetic biochar prepared from pinewood and natural hematite. Bioresour. Technol. 175, 391–395.
Wang, T., Zhang, L.Y., Li, C.F., Yang, W.C., Song, T.T., Tang, C.J., Meng, Y., Dai, S., Wang, H.Y., Chai, L.Y., Luo, J., 2015b. Synthesis of core-shell magnetic Fe_3O_4@ poly(m-Phenylenediamine) particles for chromium reduction and adsorption. Environ. Sci. Technol. 49, 5654–5662.
Wang, X.S., Chen, L.F., Li, F.Y., Chen, K.L., Wan, W.Y., Tang, Y.J., 2010. Removal of Cr (VI) with wheat-residue derived black carbon: reaction mechanism and adsorption performance. J. Hazard Mater. 175, 816–822.
Wang, Y., Liu, D.F., Lu, J.B., Huang, J., 2015c. Enhanced adsorption of hexavalent chromium from aqueous solutions on facilely synthesized mesoporous iron-zirconium bimetal oxide. Colloids Surf., A 481, 133–142.
Williams, A.G.B., Scherer, M.M., 2004. Spectroscopic evidence for Fe(II)–Fe(III) electron transfer at the iron Oxide–Water interface. Environ. Sci. Technol. 38, 4782–4790.
Wu, J., Lin, G., Li, P., Yin, W., Wang, X., Yang, B., 2013. Heterogeneous Fenton-like degradation of an azo dye reactive brilliant orange by the combination of activated carbon-FeOOH catalyst and H(2)O(2). Water Sci. Technol. 67, 572–578.
Wu, P.X., Li, S.Z., Ju, L.T., Zhu, N.W., Wu, J.H., Li, P., Dang, Z., 2012. Mechanism of the reduction of hexavalent chromium by organo-montmorillonite supported iron nanoparticles. J. Hazard Mater. 219, 283–288.
Xiao, Q., Sun, Y., Zhang, J., Li, Q.J., 2015. Size-dependent of chromium (VI) adsorption on nano alpha-Fe_2O_3 surface. Appl. Surf. Sci. 356, 18–23.
Yang, J., Zhong, L., Liu, L., 2017a. Chromium (VI) reduction in the nano- or micron-sized iron oxide – citric acid systems: kinetics and mechanisms. J. Environ. Chem. Eng. 5, 2564–2569.
Yang, T., Meng, L., Han, S., Hou, J., Wang, S., Wang, X., 2017b. Simultaneous reductive and sorptive removal of Cr(VI) by activated carbon supported β-FeOOH. RSC Adv. 7, 34687–34693.
Yilmaz, M., Bayramoglu, G., Arica, M.Y., 2005. Separation and purification of lyso-zyme by Reactive Green 19 immobilised membrane affinity chromatography. Food Chem. 89, 11–18.
Zhong, J.W., Yin, W.Z., Li, Y.T., Li, P., Wu, J.H., Jiang, G.B., Gu, J.J., Liang, H., 2017. Column study of enhanced Cr(VI) removal and longevity by coupled abiotic and biotic processes using Fe-0 and mixed anaerobic culture. Water Res. 122, 536–544.
Zhong, L.Y., Yang, J.W., 2012. Reduction of Cr(VI) by malic acid in aqueous Fe-rich soil suspensions. Chemosphere 86, 973–978.
Zhuang, L.Z., Li, Q.H., Chen, J.S., Ma, B.B., Chen, S.X., 2014. Carbothermal preparation of porous carbon-encapsulated iron composite for the removal of trace hex-avalent chromium. Chem. Eng. J. 253, 24–33.